

# Condensation Phenomena in Nano-Pores - a Monte Carlo Study

Raja Paul<sup>1</sup>, Heiko Rieger<sup>1</sup>

<sup>1</sup>*Theoretische Physik, Universität des Saarlandes, 66041 Saarbrücken, Germany.*

The non-equilibrium dynamics of condensation phenomena in nano-pores is studied via Monte Carlo simulation of a lattice gas model. Hysteretic behavior of the particle density as a function of the density of a reservoir is obtained for various pore geometries in two and three dimensions. The shape of the hysteresis loops depend on the characteristics of the pore geometry. The evaporation of particles from a pore can be fitted to a stretched exponential decay of the particle density  $\rho_f(t) \sim \exp[-(t/\tau)^\beta]$ . Phase separation dynamics inside the pore is effectively described by a random walk of the non-wetting phases. Domain evolution is significantly slowed down in presence of random wall-particle potential and gives rise to a temperature dependent growth exponent. On the other hand roughness of the pore wall only delays the onset of a pure domain growth.

PACS numbers: 64.60-i, 81.07-b, 47.55.Mh, 75.40.Gb

## I. INTRODUCTION

Adsorption and desorption isotherms of a gas condensed into nano pores show hysteresis and have become very a useful tool for the classification of porous materials [1, 2, 3]. Due to the effect of surface tension the formation of meniscii inside the pore is delayed on the desorption branch, resulting in a non-vanishing hysteresis area of the sorption isotherms. A theoretical analysis and detailed description of the early research on this phenomenon is described in a review by Everett [4]. Recent investigation from a point of view of the stability of adsorbed multilayers [5] and other [6, 7, 8] analytical and numerical approaches together with density functional theory also proposed that the hysteresis phenomenon is an intrinsic property of the phase transition in a single idealized pore and arises from the existence of metastable states.

Hysteresis in real materials is the collective phenomena involving interconnected network of simple pores [9, 10]. However, quite recently it has been shown by numerical analysis [11] and experiments [12, 13, 14] that hysteresis can occur in isolated pores also. Moreover the shape of the hysteresis loops are influenced by the characteristic features of the pore geometry. In this paper, using extensive Monte Carlo simulations, we intend to characterize the sorption isotherms for different pore geometries and compare our results directly to the experimental observations.

Furthermore, we study the phase separation kinetics of a binary liquid in nano-pores at low temperatures. Previous work [15, 16, 17] showed that a binary liquid, unlike Ising-like complete phase separation, does not separate into two phases completely. Instead the adsorbed material forms many small domains far below the co-existence region. An explanation for this behavior has been suggested on the basis of random-field Ising model [18, 19, 20]. On the contrary we found in case of a single-pore model with no randomness, confinement in a small pore slows down domain growth in certain regions of the wetting phase diagram [21] and as a result macroscopic

phase separation is not observed on short time scales. Moreover the late stage domain evolution, obtained from a two point correlation function  $C(r, t)$  follows the same Lifshitz-Slyozov [22] growth law of  $t^{1/3}$ . Unlike earlier research [23] of domain evolution in porous networks, we concentrate on a single pore which is more applicable for systems with low porosity (Si mesopores [14]). Moreover, randomness in terms of irregular pore structure or presence of impurity atoms in the pore wall, which is inherent in real systems, may have drastic effect on the domain growth.

In this paper we focus on a single pore. An average over many isolated pores corresponding to an assembly of non-interconnected (unlike Vycor) pores can be experimentally developed [14] out of a B-doped Si wafer via electrochemical etching. The structure of the rest of the paper is as follows. First we overview, in section II, the theoretical model and the Monte Carlo technique that we use in our simulation. In section III A, we discuss the Hysteresis phenomenon for different pore geometries in 2 and 3 dimensions and discuss how one can differentiate the pore structure from the hysteresis loops. In section III B, we focus on the evaporation of particles from the pore and discuss how the density in the pore reaches a new equilibrium value. Sections III C, D are entirely devoted to the domain evolution in the pore environment where we propose a random-walk picture of the domain growth above a critical size comparable to the pore diameter. Then we perform a quantitative study of growth phenomenon for a simple pore as well as for pores with defects. Finally section IV finishes the paper with a discussion.

## II. SIMULATION MODEL

A standard model for a binary liquid mixture, is the Ising lattice-gas model with spin occupancy variables  $\sigma_i$

= 0, 1 governed by the Hamiltonian:

$$\mathcal{H} = -W_{pp} \sum_{bulk(i,j)} \sigma_i \sigma_j - W_{wp} \sum_{i \text{ n.n. of wall}} \sigma_i, \quad (1)$$

where  $W_{pp}$  and  $W_{wp}$  are the particle-particle and wall-particle couplings respectively. We denote an occupied site as a particle and an empty site as a vacancy. Experimental observations suggest that in case of a glass(Si) adsorbent, the pore wall has a very strong affinity towards the adsorbed gases, which implies  $W_{wp} > W_{pp}$ . Most of our simulations, unless otherwise specified, are performed at a fixed ‘‘wettability’’  $W_{wp}/W_{pp} = 1.5$ . A change in this value does not qualitatively affect our results as long as  $W_{wp} > W_{pp}$ . The geometry of the pores is chosen to be a rectangle of size  $L \times h$  in two dimension and parallelepiped of size  $L \times h \times h$  in three dimension with  $h \ll L$ . Standard conserved order parameter dynamics(Kawasaki) is employed to study the diffusion and the domain growth kinetics in the nano pores. Nearest neighbor spins  $\sigma_i$  and  $\sigma_j$  are exchanged with Metropolis acceptance probability

$$P(\{\sigma\} \rightarrow \{\sigma'\}) = \min \left[ 1, \frac{\exp(-\beta\mathcal{H}\{\sigma'\})}{\exp(-\beta\mathcal{H}\{\sigma\})} \right], \quad (2)$$

where  $\sigma$  and  $\sigma'$  represents the old and new spin configuration respectively. To improve the speed of simulations we always choose a particle with unit probability and define 1 MC step containing a number of trial-updates that is equal to the number of particles present in the system.

### III. NUMERICAL RESULTS

#### A. Hysteresis

To study hysteresis in the adsorption/desorption process within a pore we attach one or two reservoirs depending upon the geometry of the pore. To avoid asymmetric diffusion into the pore, no periodic boundary condition is applied between the reservoirs. The particle density in the reservoirs is kept constant by adding(removing) particle at a randomly chosen position in the reservoir as soon as a particle diffuses into the pore(reservoir). A snapshot of the hysteresis phenomenon for a simple pore geometry in  $2d$  is shown in Fig. 1. Initially, both the pore and the reservoirs are kept empty. The density of particles in the reservoirs( $\rho_{res}$ ) are then slowly increased. Particles are immediately adsorbed and form a single layer along the pore walls. At this stage the density in the pores( $\rho_f$ ), rises sharply to a non-zero value which corresponds to the first jump of adsorption isotherms(Fig. 2). Then  $\rho_f$  forms a long plateau until two semicircular(or hemispherical in  $3d$ ) meniscii(a meniscus for one-end open pore) are formed somewhere in the middle of the pore at a high reservoir density and move apart from each other to fill the entire pore; a second jump in  $\rho_f$  is observed. We

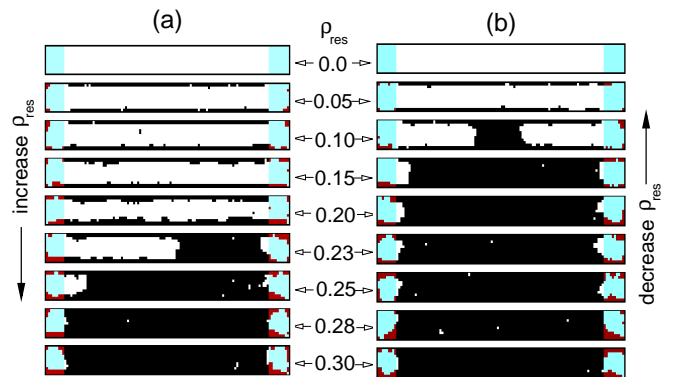


FIG. 1: Snapshots of the hysteresis in a simple nano-pore of size  $L = 100$  and  $h = 11$  at temperature  $T = 0.3$ . The shaded regions and the black spots on both sides of the pore are respectively the attached reservoirs and the particles in it. For each value of  $\rho_{res}$  the system is equilibrated up to  $t = 2^{22}$ . Snapshots (a) correspond to the adsorption and (b) correspond to the desorption isotherms.

call this complete pore filling and further increase in  $\rho_{res}$  does not change  $\rho_f$ .

Next, we slowly decrease the reservoir density and record the corresponding filling fraction  $\rho_f$  after the system is equilibrated. On desorption, however at a much smaller reservoir density  $\rho_{res}$ , we see the semicircular meniscii to form on the open ends of the pore, followed by a sharp fall in the pore density  $\rho_f$ , as the meniscii approaches towards each other. Finally the desorption curve follows the same path as that of the adsorption. Since the diffusion occurs very slowly into the pores, a long waiting time  $t_w$  is needed to equilibrate the whole system for each value of  $\rho_{res}$ .

Our simulation results are shown in Fig. 2 where column (a) and (b) shows the hysteresis in 2 and 3 dimensions respectively. The simulations are performed with systems of length  $L = 100$  and  $50$  at temperatures  $T = 0.3, 0.6$  in  $2d$  and  $3d$  respectively. Reservoir lengths are kept fixed at  $L_r = 10$ . Ink-bottle pores are equally divided into two parts; one with the narrow tube of diameter  $h_1$  and the other is relatively wider sack with diameter  $h_2$ . To make sure that pore density  $\rho_f$  does not change any more, each data point of the sorption-isotherms is equilibrated for  $t_w = 2^{22}$  time steps. Finally for each hysteresis loop data are averaged over 50 ensembles. It is evident from the sorption branches of II-IIIa,b, that they are much steeper than in Ia,b. This is due the formation of two meniscii on both sides of the pore, which accelerate the filling and emptying procedure. Such characteristic feature distinguishes between a one-end open and both-end open pore. Further, an increase in pore diameter requires a higher reservoir density to initiate the formation of meniscii, which effectively delays the onset of adsorption saturation. As a result the the loop area for bigger pore is also increased as shown in IIa,b and IIIa,b. This features can be used to compare pores of different sizes.

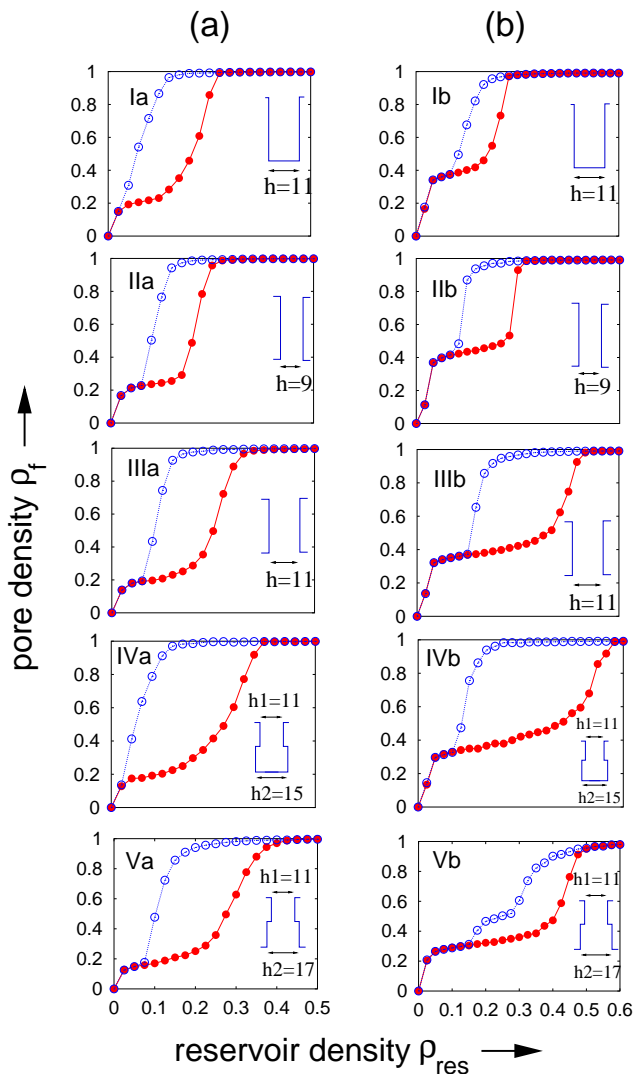


FIG. 2: Adsorption (filled circles) and desorption (empty circles) isotherms for nano pores. **(a)**: Filling fraction  $\rho_f$  of the pore as a function of the reservoir density  $\rho_{res}$  in 2 dimension. The equilibration time  $t_w$  for each data point  $2^{22}$ . Ia has one reservoir of length 10 attached to the open end. IIa, IIIa and IVa has 2 reservoir attached on both sides. **(b)**: Hysteresis isotherms in 3 dimension. Equilibration time  $t_w = 2^{22}$ , pore length  $L = 50$  and reservoir length is 10. For each hysteresis isotherm data are averaged over 50 disorder samples.

In experiments [14] one observes a two step decrease of the desorption isotherms corresponding to ink-bottle pores. Our data, as shown in figure Vb, for a both-end open pore in 3d of similar geometry, agrees quite well with the experimental predictions. The two step decrease of the desorption isotherm arises from the sequential emptying of the different sections (of diameter  $h_1$  and  $h_2$ ) of the pore. The heights of the two steps suggest the wider section of the pore emptied earlier than the smaller section. However, ink-bottle pores in figure IVa,b (2d-both end open) and Va (3d-one end open) do not exhibit such special characteristics. Absence of this feature may be

due to a small temperature or a small system size with insufficient  $h_2/h_1$  ratio.

## B. Evaporation

If a partially or completely filled pore is kept in vacuum, the density inside it decreases with time. This is what we call evaporation and investigate it for different pore geometries. In experiments [14] one measures the vapor pressure change inside a previously equilibrated pore subject to the pressure variation in the reservoir. However, we carry out the simulation in a slightly different way by keeping the initial pore density just above the desorption threshold.

To study the variation in pore density  $\rho_f$  as a function of time we fill pores completely and allow it to evaporate in an empty reservoir (vacuum). The change in  $\rho_f$  has been recorded as a function of time  $t$ . Decay of the pore density can be very well described by a stretched exponential law,

$$\rho_f(t) \sim \exp[-(t/\tau)^\beta]. \quad (3)$$

The simulation is carried out in pores with both simple and ink-bottle geometry. For simple pore we study the evaporation at temperature  $T = 0.4$ , for systems with  $L = 128, 256, 400, 512$  and  $h = 7$  and finally average over 50 ensembles. The pore density  $\rho_f$  as a function of time  $t$  is plotted in Fig. 3(a) in a log-linear scale. It is noticed that a pure stretched exponential decay is found only above a certain value of the pore filling fraction as shown by continuous lines. These values of  $\rho_f$  are nothing but the ratio between the number of surface to bulk molecules and decreases as  $L$  becomes larger. The surface molecules, are attached rather strongly ( $W_{wp} > W_{pp}$ ) to the walls and slow down the evaporation rate for a while but finally drop off suddenly to zero. As the length of the system is increased, the particles deep inside the pore requires much more trial attempts to diffuse till the open end which effectively increases the evaporation time for longer pores. This leads to the decay exponent  $\beta$  to decrease with  $L$ , as shown in the inset of (a).

A similar study in case of ink-bottle pores was carried out with systems of fixed  $L = 200$  and  $h_1 = 7$  for different values of  $h_2 = 7, 21, 35, 49$  as shown in Fig. 3(b). The temperature is kept fixed at  $T = 0.4$  and data are averaged over 50 ensembles. Like the previous case, here also,  $\rho_f$  shows a pure stretched exponential decay above a certain value, which becomes smaller as  $h_2$  is increased. Moreover the effective length ( $L + h_2$ ) of the pore increase with  $h_2$  results in the decay exponent  $\beta$  (inset of (b)) to drop off similarly to the simple pore.

A further analysis (not shown) on both simple and ink-bottle pore shows that  $\beta$  is independent of the temperature.

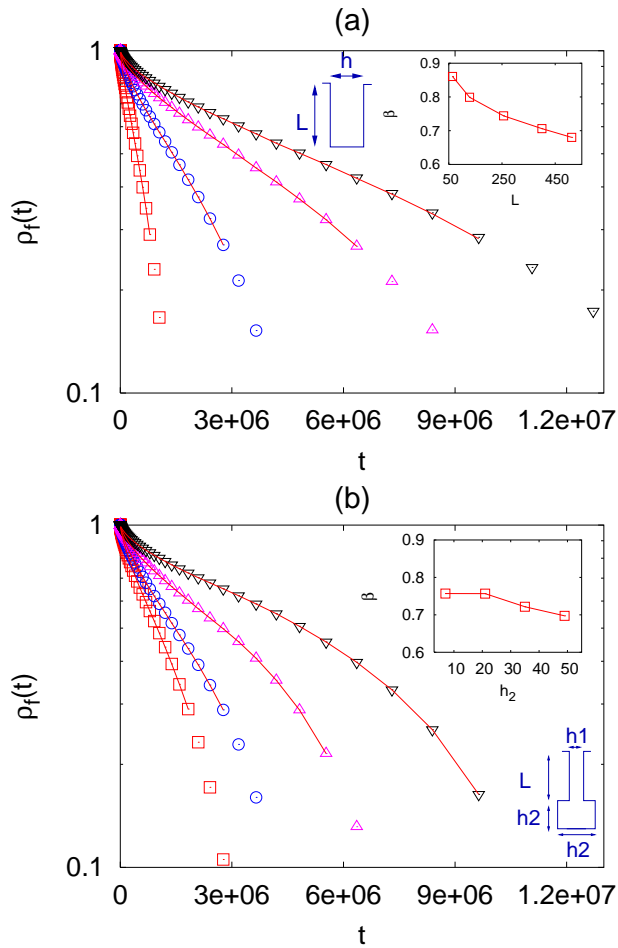


FIG. 3: **(a)**: Evaporation from simple pores of diameter  $h = 7$  and different lengths  $L = 128, 256, 400$  and  $512$  from left to right at temperature  $T = 0.4$ . Data for the filling fraction  $\rho_f(t)$  are shown in a log-linear scale - note that the decay is initially slower than exponential. The full line connects the data points that can very well be fitted to a stretched exponential with the exponent  $\beta$  given in the *inset*. **Inset**: The decay exponent  $\beta$  as a function of the pore length  $L$ . **(b)**:  $\rho_f(t)$  for ink-bottle pores of fixed length  $L = 200$ , tube diameter  $h_1 = 7$  at  $T = 0.4$  for different sack width  $h_2 = 7, 21, 25, 49$  from left to right. The decay law is similar to the simple pores. **Inset**:  $\beta$  as a function of  $h_2$ .

### C. Domain evolution and Random Walks

In this section we study the temporal evolution of domain structures inside pores starting with a random (high temperature) initial configuration of given density. Now we use periodic boundary conditions between the two ends of the pore and the total number of particle is conserved. Fig. 4(a), shows the domain structure-profile at different time steps when the system is quenched to  $T = 0.3$  from  $T = \infty$ . Fig. 4(b) is the snap-shot of a cut along the pore axis. The black regions correspond to the occupied sites and are called “particle-domains”, whereas empty white regions are termed “blobs”.

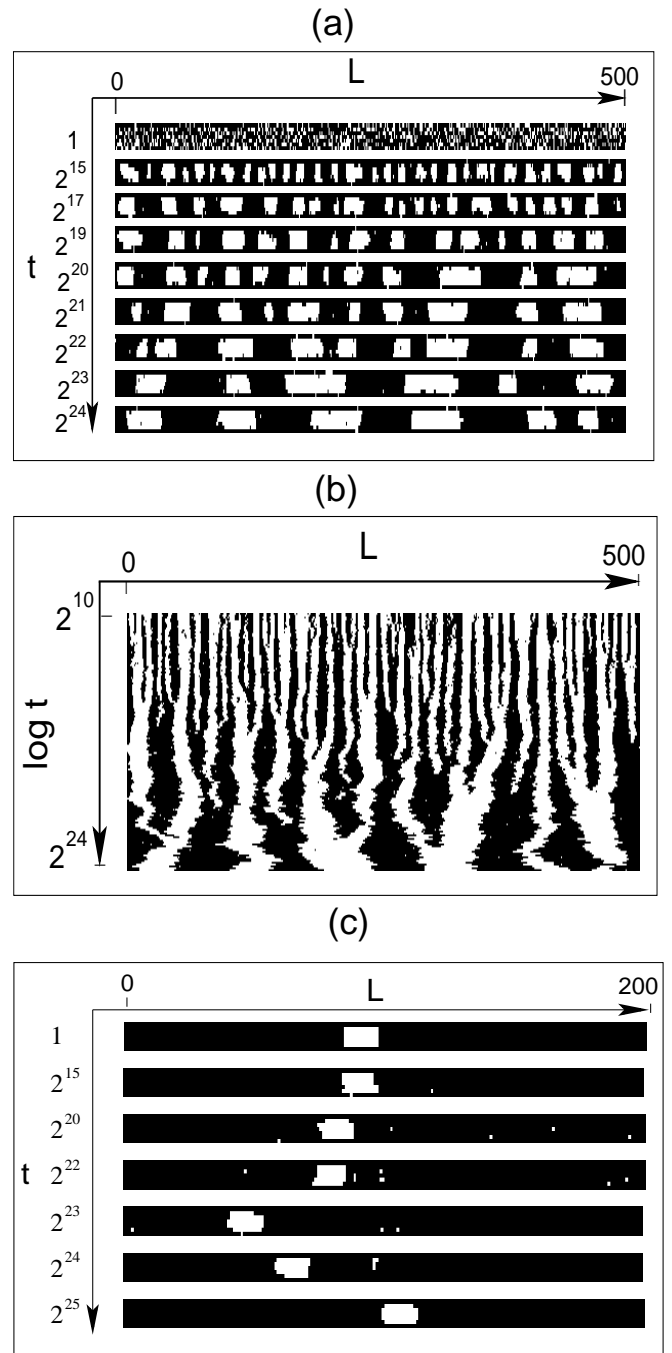


FIG. 4: **(a)**: Domain evolution in nano-pores. Figures are produced by taking snap-shot for a system of length  $L = 300$  and height  $h = 7$  at temperature  $T = 0.3$ . **(b)**: Axial snapshot of the domains for the same system in Fig. (a). A horizontal cut through the figure at any instant  $t$  will give the location and size of domains/blobs along the axis of the pore. The time is plotted in logarithmic scale. **(c)**: Time evolution of a single rectangular blob of linear size  $l_b = 13$  in a pore of dimension  $200 \times 7$  at  $T = 0.3$ .

In the initial stage, the growth is dominated by nucleation and spinodal decomposition. As soon as the domain- or the blob-size becomes comparable to the diameter of the pore, the above two mechanisms do not work any more. Transverse directional growth is completely stopped because of the pore wall and the horizontal movement of the blobs is slowed down by the presence of the particle-domains.

The snapshots in Fig. 4 confirm that the random motion of the blobs plays an important role in the late stage of growth. A closer look to Fig. 4(b), which is horizontally the occupancy along the pore-axis and vertically time in log scale, shows in the late stage, the blobs move to and fro along the axis of the pore and penetrate through the particle-domains to coalesce with the neighbors. During this process it also transfers a holes(vacancies, white regions) from its surface to the neighboring blobs.

To elucidate the random motion, we study the time evolution of a single blob as shown in Fig 3(c). Initially it is a perfect rectangle of linear size( $l_b$ ) comparable to the pore diameter( $h$ ) and placed in the center of the pore. The temperature is kept fixed at  $T = 0.3$ . The system is allowed to evolve and the mean square deviation  $\langle x^2(t) \rangle$  of the center of mass(CAM) of the blob along the axis of the pore is measured at each time step. Since the boundary of the blob perpendicular to the wall, fluctuates very rapidly, the true COM may not lie on the geometrical axis of the pore. In this case we trace the actual COM and project it on to the axis. The size of the blob has to be chosen large enough to avoid disintegration of the main blob.

Since we start with an exactly rectangular blob, a true random-walk motion is not immediately observed. In the early stages, the blob walls, perpendicular to the pore axis roughens, leading to  $\langle x^2(t) \rangle \sim t^{2/3}$  as in surface roughening described by the KPZ-equation [24]. At late stages ( $t > 10^4$ ), the blob performs a random walk with a blob-size dependent diffusion constant  $\mathcal{D}(l_b)$ ,

$$\langle x^2(t) \rangle = \mathcal{D}(l_b) t. \quad (4)$$

Fig. 5(a), shows the mean square displacement  $\langle x^2(t) \rangle$  of the COM of blobs with  $l_b = 11, 15, 19, 23, 27, 31, 35, 39$  as a function of time  $t$ . For each values of  $l_b$  the simulation is carried out in a system with fixed  $L = 200$ ,  $h = 7$  at temperature  $T = 0.3$  and finally averaged over 1000 ensembles. It is evident from the figure that the onset of a true random-walk is delayed for bigger blobs. A scaling form for both small and large time scale regime is,

$$\langle x^2(l_b, t) \rangle \propto \tau^\theta(l_b) f(t/\tau(l_b)) \quad (5)$$

with

$$f(x) \sim \begin{cases} x^\theta & \text{for } x \ll 1 \\ x & \text{for } x \gg 1. \end{cases} \quad (6)$$

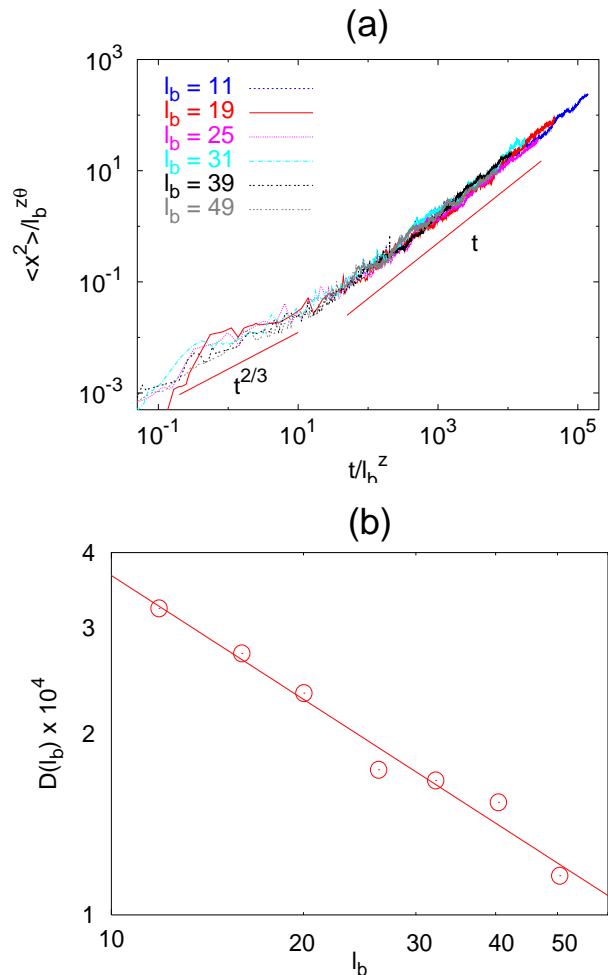


FIG. 5: (a): Mean-square deviation of blobs of size  $l_b = 11, 15, 19, 23, 27, 31, 35, 39$  for a system size  $L = 200$ ,  $h = 7$  and the temperature  $T = 0.3$ . (b): Shows the power law decay of the diffusion constant  $\mathcal{D}(l_b)$  for different blob sizes. The exponent is found to be  $\gamma = 0.68$ .

Assuming,  $\tau(l_b) \sim l_b^z$ , from Eq. 5, one can write for large time  $t \gg \tau$ ,

$$\langle x^2(l_b, t) \rangle \propto l_b^{z(\theta-1)} t, \quad (7)$$

which readily gives,

$$\mathcal{D}(l_b) \sim l_b^{-z(1-\theta)} = l_b^{-\gamma}. \quad (8)$$

The scaling form in Eq. 5 gives quite reasonable data collapse for  $\theta = 2/3$  and  $z = 2$ , as shown in Fig. 5(a). Substituting these value in Eq. 8 we obtain the value of  $\gamma = 2/3$ . Diffusion constant  $\mathcal{D}$  evaluated from the asymptotic behavior [c. f. Fig 5(a)] is plotted in Fig 5(b). From the slope of  $\mathcal{D}$  vs.  $l_b$  curve in log-log scale we estimate the  $\gamma = 0.68$  which agrees quite well with the previous value  $2/3$ , obtained from the scaling. Note that the relation  $\mathcal{D} \propto 1/l_b^{2/3}$  deviates from the naive expectation  $\mathcal{D} \propto k_B T \eta / l_b$  [21, 25], where  $k_B$ ,  $T$ ,  $\eta$  are the Boltzmann' constant, temperature and viscosity coefficient of the medium respectively.

### D. Correlation function and Domain growth exponent

An alternative way to study domain growth is via the measurement of the correlation function  $C(r, t)$  along the axis of the nano-pore in a similar fashion as in the Ising model.

$$C(r, t) = \langle S(0, t)S(r, t) \rangle - \langle S \rangle^2, \quad (9)$$

where  $S(r, t) = 2\sigma(r, t) - 1$ , the Lattice gas-variable, takes the values  $-1, 1$  for  $\sigma = 0, 1$  respectively. Due to this transformation,  $C(r, t)$  falls off with  $r$  in an oscillatory fashion, as is shown in the *inset* of Fig. 6(a). Following Huse [27], we also define the length scale or the typical domain size  $R(t)$  of the system as the position of the first zero of  $C(r, t)$ . Calculating  $C(r, t)$  using Eq. 9 we extract  $R(t)$  by fitting the three or four points in  $C(r, t)$  closest to its first zero to a quadratic function of  $r$  and defining  $R(t)$  as the value of  $r$  for which the function vanishes. At very late stage ( $t > \tau(T)$ ), the asymptotic domain size  $R(t)$  grows as a power-law,

$$R(t) \sim t^{1/\psi}, \quad (10)$$

where  $1/\psi$  is the growth exponent. The onset of such a power law regime shifts towards the early time scales as the temperature is increased.

We studied the domain growth for both (i) simple and (ii) complex pores. By “simple” we specify a pore with no geometrical defects in the wall and has a fixed value of  $W_{wp}$ . “Complex” pores are further subcategorized into (ii)-a: simple pore with random  $W_{wp} \in [0, 1.5]$  and (ii)-b: pore with fixed  $W_{wp}$  but geometrical defects along the wall. Let us discuss about the “simple” pores first. The domain evolution in this case studied with a system of length  $L = 500$  and height  $h = 7$  at different temperature  $T = 0.25, 0.3, 0.35, 0.4$ . For each temperature we averaged over 300 ensembles. The average length scale or the domain size  $R(t)$  as a function of the time  $t$  is plotted in the Fig. 6(a). The growth exponents  $1/\psi$ , extracted from this figure, for different values of temperatures, is shown by upper curve in Fig. 6(b). This exponent appears to be  $1/\psi \sim 1/3$  independent of the temperature. On the other hand, for the case (ii)-a with defects in terms of random wall-particle coupling  $W_{wp} \in [0, 1.5]$ , we carried out a similar kind of study as described above. It is observed that the growth process is drastically slowed down by the pinning-effect [28] of non-wetting sites located randomly in the pore walls. And as a consequence the exponents are also reduced quite significantly and found to have a temperature dependence as well, as shown in the bottom of Fig. 6(b).

It is also noticed, for the case (ii)-b, that a periodic structure-defect of the pore wall has a strong influence on the domain growth. In Fig. 7(a) we demonstrate the effect of a variable periodicity  $R_L$  for system of length  $L = 512$  with two fixed pore diameters  $h_1 = 9, h_2 = 15$ . The simulations are done at a constant temperature

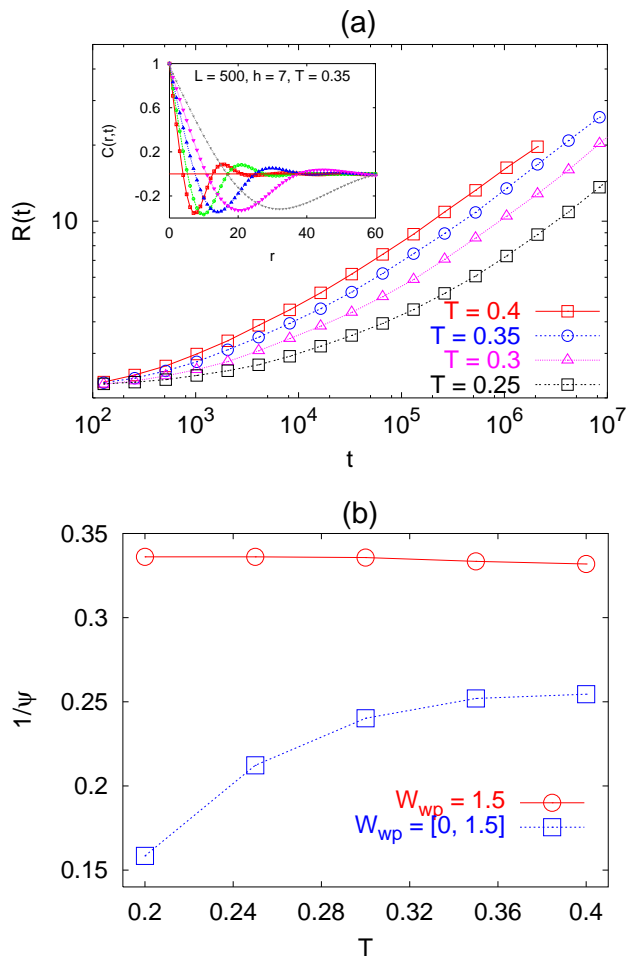


FIG. 6: (a): Average domain size  $R(t)$  as a function of time  $t$  for different quenches to  $T = 0.4, 0.35, 0.3$ . The system size  $L = 500, h = 7$  and the density  $\rho_f = 0.7$ . **Inset** : Correlation function  $C(r, t)$  at various times  $t$  after a quench to  $T = 0.35$ . The domain size  $R(t)$  is defined as the distance of the first zero from the origin. (b): Growth exponent  $1/\psi$  plotted against the temperature  $T$ . The upper curve, for fixed  $W_{wp}$ , is almost a constant with  $T$ , whereas the lower one, for random  $W_{wp}$ , shows a steep decrease for smaller values of  $T$ .

$T = 0.35$  and for each value of  $R_L$ , the data are averaged over 300 ensembles. Domains grow quite fast in either part of the  $h_1$  or  $h_2$  diameters, but finally due to the bottle-neck effect it becomes extremely hard to transfer the particle-domains or blobs from one side of the narrow part (diameter  $h_1$ ) of the pore to the other. Consequently the growth process is slowed down. But in the late stage, when the domain size  $R(t)$  becomes comparable to the periodicity  $R_L$ , the blobs are in similar environment like in a simple pore and a true power law growth sets on. As a result a longer periodicity corresponds to a late initiation of the power law growth. We carried out the simulation for 4 different values of periodicity  $R_L = 4, 8, 16, 32$  and for the first 3 values of  $R_L$  we found a late stage growth exponent  $1/\psi = 0.33$ , but for  $R_L = 32$ , the power law growth is not yet initiated. For such a

large periodicity one certainly has to wait extremely long. Further, we carried out a similar study by varying the pore diameter  $h_2$  while keeping the periodicity  $R_L$  fixed. The numerical data are obtained with a system of  $L = 512$ ,  $h_1 = 9$ ,  $R_L$ ,  $T = 0.35$  and  $h_2 = 13, 15, 17, 23$ . Finally for each value  $h_2$  we average over 300 ensembles. The domain size  $R(t)$  is plotted in Fig. 7(b). In the initial stage of the growth, as described above, the domain grows quite independently in either part of the pore with  $h_1$  and  $h_2$  diameters. A true power law growth, which starts after  $R(t) \geq R_L$ , is slightly delayed for larger  $h_2$ . As described above, to attain a pore environment similar to the simple pore it is necessary to equilibrate the top and bottom of the wider part ( $h_2$ ) of the pore which takes longer as  $h_2$  is increased. Finally, the growth exponent extracted in the late stage, found to have the same value  $1/\psi = 0.33$ , as that of the pure model.

#### IV. DISCUSSION

Using extensive Monte Carlo simulations we have shown how hysteresis arises in nano-pores for different pore structures. The characteristics of the sorption branches are influenced by the shape and size of the pore geometry. Since the hysteresis in nano-pores occur due to diffusion, the temperature has to be chosen very carefully to avoid slow diffusion rate at low temperatures or vanishing hysteresis-loop at high temperatures. Absence of two-step desorption branch in  $2d$  ink-bottle pores may be due to the effect of a small temperate as found in the experiment [14]. Choice of pore diameters for one-end open ink-bottle geometry is also an important factor. Because of surface tension effect, a large curvature ratio  $\frac{1}{h_1}/\frac{1}{h_2}$ , can cause a huge pressure difference between the narrow and wide parts of the pore. Increase in curvature corresponds to a decrease in vapor pressure; described by the Kelvin equation. As an effect if the narrow part of the pore is filled early, can block the particle to diffuse into the wider part, unless a very high density is reached in the reservoir.

The stretched exponential decay of the pore density  $\rho_f(t)$  also agrees qualitatively with the experiments [14]. One simple reason of such a behavior of  $\rho_f(t)$  could be due to the formation of meniscus at the open end of the pore which eventually restricts the rate of evaporation depending upon the radius of its curvature.

For the phase separation of binary liquids in the pore environment, model **B** [29] corresponding to dynamics with conserved order parameter, is not well suited, as it does not account for the transport of the order parameter by hydrodynamic flow. Modifications to model **B** by adding an ‘‘advection’’ term describes the system quite well [26].

Late stage coarsening in pore system that we studied is effectively driven by two mechanisms:(1)Transfer of holes

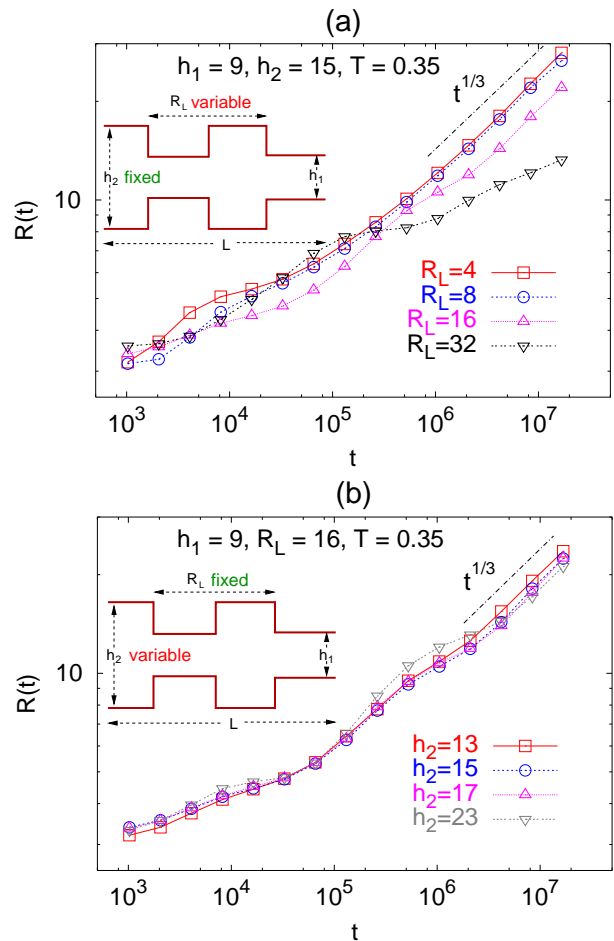


FIG. 7: (a): Average domain size  $R(t)$  of a defected pore-wall for periodicities  $R_L = 4, 8, 16$  and  $32$  at temperature  $T = 0.35$ . The system has fixed length  $L = 512$  and diameters  $h_1 = 9$  and  $h_2 = 15$ . Domain growth slows down for larger periodicity. (b):  $R(t)$  for different pore diameters  $h_2 = 13, 15, 17$  and  $23$  at fixed  $L = 512$ ,  $h_1 = 9$ ,  $R_L = 16$ , and  $T = 0.35$ . The domain growth remain constant while varying  $h_2$ .

from the surface of one blob to a neighboring blob and (2) the transfer of particles from one side of the blob to the other along the pore wall. Owing to the first mechanism a blob shrinks and the neighboring blobs grow, whereas due to the second one a blob moves to and fro as a whole and coalesce with another. Our numerical study for a single blob (section III(C)), account for the contribution arises from (2) only and gives rise to the diffusion constant  $\mathcal{D} \sim l_b^{-2/3}$  of a blob of size  $l_b$ . The first mechanism modifies the single-blob diffusion constant in a non-trivial way, which is difficult to estimate. Finally, the superposition of random motion of blobs due to mechanism (2) and the hole transfer mechanism in (1) leads to a late-stage growth law  $R(t) \sim t^{1/3}$ , independent of their individual contributions.

The domain growth exponent  $1/\psi$  is significantly decreased in presence of random wall-particle potential  $W_{wp}$  which in practice is due to the effect of impurity

atoms at the pore walls. The temperature dependence of the exponent may come from a logarithmic scaling [28] of barrier energy of the domains. On the other hand geometrical defects appear to slow down the growth process only in the early time regime. But in the late stage, as the blob size becomes larger than the wave length of the geometrical disorder, which in this case is the periodicity of the wall-defect, the domain growth shows a pure

behavior.

### Acknowledgments

This work was financially supported by the Deutsche Forschungsgemeinschaft (DFG), SFB277.

- 
- [1] F. Rouquerol, J. Rouquerol and K. Sing, *Adsorption by Powders and Porous Solids*, Academic Press: New York, 1999, Chapter 7.
- [2] K. S. W. Sing, D. H. Everett, R. A. W. Haul, L. Moscou, R. A. Pierotti, J. Rouquerol, T. Siemieniewska, *Pure Appl. Chem.* **57**, 603 (1985).
- [3] L. D. Gelb *et al.*, *Rep. Prog. Phys.* **62** 1573 (1999).
- [4] D. H. Everett, in *The Solid Gas Interface*, edited by E. A. Flood (Marcel Dekker, New York, 1967), Vol. 2, p. 1055.
- [5] W. F. Saam and M. W. Cole, *Phys. Rev. B* **11**, 1086 (1975)
- [6] F. Celestini, *Phys. Lett. A* **288**, 84 (1997).
- [7] A. Papadopoulou, F. van Swol and U. Marini Bettolo Marconi, *J. Chem. Phys.* **97**, 6942 (1992).
- [8] R. Evans, U. Marini Bettolo Marconi and P. Tarazona, *J. Chem. Phys.* **84**, 2376 (1986).
- [9] R. A. Guyer and K. R. McCall, *Phys. Rev. B* **54**, 18 (1996)
- [10] G. Mason, *Proc. R. Soc. London, Ser. A* **415**, 453 (1988)
- [11] L. Sarkisov and P. A. Monson, *Langmuir* **17**, 7600 (2001) and Ref. therein.
- [12] J. H. Page, J. Liu, B. Abeles, H. W. Deckman and D. A. Weitz, *Phys. Rev. Lett.* **71**, 1216 (1993)
- [13] P. Huber and K. Knorr, *Phys. Rev. B* **60**, 12657 (1999)
- [14] D. Wallacher, N. Künzner, D. Kovalev, N. Knorr and K. Knorr, *Phys. Rev. Lett.* **92**, 195704 (2004)
- [15] M. C. Goh, W. I. Goldberg and C. M. Knobler, *Phys. Rev. Lett.* **58**, 1008 (1987)
- [16] S. B. Dierker and P. Wiltzius, *Phys. Rev. Lett.* **58**, 1865 (1987)
- [17] M. Y. Lin, S. K. Sinha, J. M. Drake, X.-l. Wu, P. Thiya-grajan and H. B. Stanley, *Phys. Rev. Lett.* **72**, 2207 (1994).
- [18] F. Brochard and P. G. de Gennes, *J. Phys. Lett.(Paris)* **44**, 785(1983)
- [19] P. G. de Gennes, *J. Phys. Chem.* **88**, 6469 (1984)
- [20] R. J. Birgeneau, R. A. Cowley, G. Shirane and H. Yosthizawa, *J. Stat. Phys.* **34**, 817 (1986)
- [21] L. Monette, A. J. Liu and G. S. Grest, *Phys. Rev. A* **46**, 7664(1992); A. J. Liu, D. J. Durian, E. Herbolzheimer and S. A. Safran, *Phys. Rev. Lett.* **65** 1897 (1990).
- [22] I. M. Lifshitz and V. V. Slyozov, *J. Phys. Chem. Solids* **19**, 35 (1961)
- [23] J. C. Lee, *Phys. Rev. B* **46**, 8648 (1992).
- [24] M. Kardar, G. Parisi and Y. C. Zhang, *Phys. Rev. Lett.* **56**, 889 (1986).
- [25] E. D. Siggia, *Phys. Rev. A* **20**, 595 (1979).
- [26] A. J. Bray, *Adv. Phys.* **51**, 481 (2002).
- [27] D. A. Huse, *Phys. Rev. B* **36**, 5383 (1987)
- [28] R. Paul, S. Puri and H. Rieger, *Europhys. Lett.* **68** 881 (2004).
- [29] P. C. Hohenberg and B. I. Halperin, *Rev. Mod. Phys.* **49**, 435 (1977).